Hindawi
Shock and Vibration
Volume 2021, Article ID 9955497, 18 pages
https://doi.org/10.1155/2021/9955497

Research Article

The Influence Mechanism of In Situ Stress State on the Stability of Deep-Buried-Curved Tunnel in Qinghai-Tibet Plateau and Its Adjacent Region

Huiqing Wang [1,2] Chengxuan Tan,[1] Chengjun Feng,[1] Peng Zhang,[1] Bangshen Qi,[1] Zhangliang Tan,[3] Jing Meng,[1] and Weijun Guo[4]

[1] *Institute of Geomechanics, Chinese Academy of Geological Sciences, Beijing 100081, China*
[2] *China Institute for Geoenvironmental Monitoring, Beijing 100081, China*
[3] *University of British Columbia, Vancouver, British Columbia, Canada*
[4] *Beijing Polytechnic College, Beijing 100042, China*

Correspondence should be addressed to Huiqing Wang; huiqing_wang@foxmail.com

Received 12 March 2021; Accepted 1 November 2021; Published 21 December 2021

Academic Editor: Shuang Li

In China, rockburst disaster occurs mostly in construction of underground engineering in Qinghai-Tibet Plateau and its adjacent region. Previous research on deep-buried tunnels has indicated that tunnels stability is related to in situ stress state. To quantify these relationships, three-dimensional finite element modeling was done to analyze the influences that the angle φ between the maximum horizontal principal stress orientation and tunnel axis, and the lateral pressure coefficient K_H, had on the tangential stress σ_θ in a deep-buried-curved tunnel. Based on the in situ stress condition in Qinghai-Tibet Plateau and its adjacent region, 50 different simulation conditions were used to analyze the relationship that φ and K_H had on σ_θ for the rock mass surrounding the tunnel. With the simulation data produced, predictive equations were generated for σ_θ as a function of φ and K_H using multivariate regression analysis. These equations help estimate σ_θ at various key positons along the tunnel boundary at Qinghai-Tibet plateau and its adjacent region. The equations were then proved by a set of typical tunnels to ensure validity. The results concluded that the change in φ has a significant impact on σ_θ, and thus, the stability of the tunnel, when $30^\circ < \varphi < 60^\circ$, with the most obvious influence being when φ is about 45°. With the equations, the rockburst potential at a certain location within a curved tunnel can be quickly estimated by calculating φ and K_H on σ_θ, without need of geo-stress background knowledge and heavy simulation, allowing for the practical value in engineering at design phase for the projects in Qinghai-Tibet Plateau and its adjacent region.

1. Introduction

Rockburst is a sudden and violent failure of the rock mass, caused by highly stressed brittle rocks and the rapid release of accumulated strain energy [1]. It has strong suddenness, randomness, and harmfulness. Frequent rockburst disasters directly affect the construction progress, threaten the safety of workers, and cause significant loss of equipment and time [2–4].

The Qinghai-Tibet Plateau is one of the most active areas of neotectonic movement in the world [5–12]. Intense tectonic activity resulted in the topography of the Qinghai-Tibet Plateau with a lot of high-altitude mountains and deep-cutting valleys. Large number of highway and railway tunnels have been or will be built inevitably in these mountainous areas [7]; thus, rockburst disasters occurred mostly in the construction of underground engineering in Qinghai-Tibet Plateau and its adjacent region [13–16]. Scholars at China and abroad have carried out research studies and obtained many valuable conclusions about the mechanism of rockburst formation, disaster effects, and preventive measures in the region

[7, 14, 17–20]. The construction of related projects has become a world problem in this complex geological environment [21].

Previous research on construction of deep-buried tunnels in areas of strong tectonic activity indicated close correlation between the stability of tunnels and in situ stress state [2, 22–24]. However, orientation and magnitude of in situ stress in such regions are very complicated due to many influencing factors including strong neotectonics activities, active faults, height difference, and so on [25, 26].

The orientation of in situ stress plays an essential factor in affecting the failure mode and stability of curved tunnels [2, 18, 27–29]. For instance, different orientations of in situ stress induce different failures types of the surrounding rock mass [30–34]. Previous research discovered that a tunnel has the highest stability when maximum horizontal principal stress orientation falls parallel with tunnel axis. In addition, the lowest stability occurs when the angle between the two is 90° [30, 32, 35].

Sufficient evidences show that lateral pressure coefficient K_H, the ratio of the maximum horizontal principal stress σ_H. and the vertical stress σ_v are also critical factors affecting stability and stress redistribution of the tunnel surrounding rock mass [22, 35–40]. Many studies devoted to explore the characteristics of fracture behaviors, failure path, and strain energy density of the deep-buried tunnel under different K_H. With small K_H, the roof and spandrel of the tunnel emancipate strain energy in long period induced spalling, and the position of initial failures is of a certain degree discreteness [35, 39]. With the increase in K_H, initial failures are mainly caused by tensile damage to roof [36]. In high-stress condition, severe rockburst activity is observed with immediate release of heavy strain energy [39]. The damage caused by the stress waves is induced from instantaneous unloading under different K_H only in the 1/3 radius propinquity of excavation perimeter [40].

In conclusion, many studies have been devoted to show that the influence of orientation of in situ stress and K_H, respectively, on the stability of the deep-buried tunnel has an important reference value. But the coupling effect of the influence mechanism of the angle φ between the maximum horizontal principal stress orientation and tunnel axis, and K_H, on the deep-buried tunnel is unclear. With the process of φ increasing from 0° to 90°, features of failure evolution are unclear, particularly when the maximum horizontal principal stress is oblique at a large angle with the tunnel axial. In addition, most of pioneer works concentrate on circle and straight-wall-top-arch tunnels [32, 41–43]. The research studies about the stress distribution and failure characteristics for curve tunnels used widely in high-speed railway remain to be explored. Therefore, although the in situ stress measurement for most deep-buried tunnels was taken before tunnel construction [15, 44, 45], rockburst still occurred frequency during construction due to lack of professional interpretation in the design stage. As a result, it is both financially and technically critical to correctly evaluate the effects of a given in situ stress state during construction.

The coupling effect of φ and K_H on the stability of the deep-buried-curved tunnel in Qinghai-Tibet Plateau and its adjacent region is investigated in this study. Stress distribution feature and the tangential stress σ_θ in the surrounding rock mass of the tunnel at five key positions (roof, floor, spandrel, corner, and sidewall) are examined. In addition, prediction equations were derived to predict σ_θ as a function of φ, K_H at key positions along the tunnel boundary via multivariate regression analysis. The equations were then tested on various tunnels in Qinghai-Tibet Plateau and its adjacent region to confirm validity. With these equations, it has become more convenient to assess σ_θ, rockburst intensity, and stability of a tunnel, all without need of tedious simulations. This will effectively serve to aid the tunnel build in planning and designing stage in Qinghai-Tibet Plateau and its adjacent region.

2. In Situ Stress Field in Qinghai-Tibet Plateau

The Qinghai-Tibet Plateau, which is formed by the strong subduction of Indian plate, extents from Altun mountains and Qilian mountains in the north, the Himalayas in the south to the Kunlun Mountains, and from the Pamirs Plateau and Karakoram Mountains in the west to the West Qinling mountains, and the Loess Plateau in the east and northeast [46]. Therefore, this study is based on the geographical space range of the Qinghai-Tibet Plateau and its adjacent region (Figure 1).

Depending on database of crustal stress in China and adjacent area, up to 2000 entries of in situ stress data measured by the hydraulic fracturing and stress relief method in Qinghai-Tibet Plateau and its adjacent region. Yao et al. [48] and Yang et al. [47] studied tectonic stress characteristics of the shallow curst, and statistical regression of measured in situ stress data with depth was analyzed. The magnitude characteristics of the maximum horizontal stress σ_H, the minimum horizontal stress σ_h, and the vertical stress σ_v changing with depth in Qinghai-Tibet Plateau and its adjacent region are shown in Figure 2(a). From the statistical regression, the relationship between σ_H, σ_h, and σ_v with depth is characterized as follows: when depth < 266 m, $\sigma_H > \sigma_h > \sigma_v$; when 266 m < depth < 1133 m, $\sigma_H > \sigma_v > \sigma_h$; when depth > 1133 m, $\sigma_v > \sigma_H > \sigma_h$. Figure 2(b) shows σ_H/σ_h variation with depth in Qinghai-Tibet Plateau and its adjacent region, which indicated that the ratio of σ_H and σ_h tends to be stable with the increase of depth. The average value of σ_H/σ_h is 1.53 in Qinghai-Tibet Plateau and its adjacent region.

3. Numerical Simulation of Three-Dimensional Stress Field

An exact analytical solution of σ_θ on the boundary of a deep tunnel with circular cross-section was carried out by Kirsch [49]; whereafter, a series of analytical solution were expanded on various conditions [50–57]. However, for a deep-buried-curved tunnel with a cross-section composed of three different radiuses, it is complicated and difficult to obtain the closed form solution of the surrounding rock mass stress.

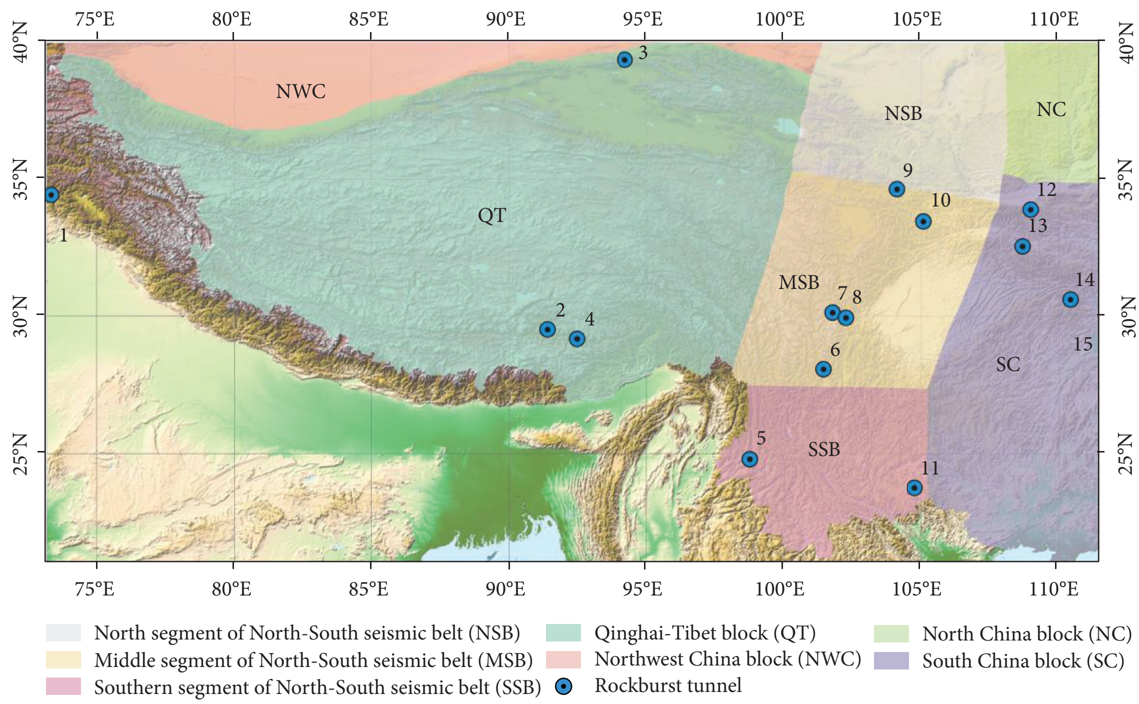

Figure 1: The range of Qinghai-Tibet Plateau and its adjacent region (adapted from [47, 48]).

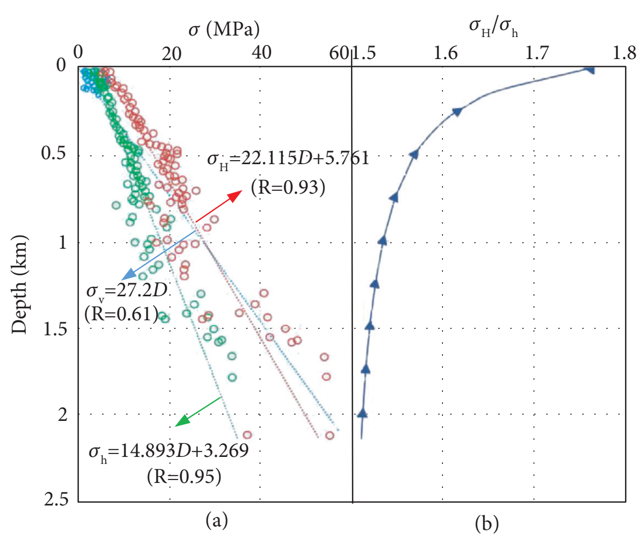

Figure 2: Measured stress variation with depth and regression equations (adapted from [47, 48]). (a) Measured stress variation with depth. (b) σ_H/σ_h variation with depth base on regression equations.

When σ_H oblique with tunnel axis, the effect of initial shear stress to stress redistribution is difficult to simulate in two-dimension stress field analyzing, resulting in a deviation with the actual simulation [32, 58]. As an effective method, three-dimensional stress field analysis by finite element approaches is applicable to solve the redistribution of σ_θ on the boundary of a deep-buried-curve tunnel. ANSYS was employed to examine the effect of in situ stress state for tunnel stability. Basic assumptions to execute the numerical simulation are summarized as follows: (1) rock mass is considered linear elastic, homogeneous, and isotropic; (2) the tunnel is infinitely long and deep-buried; (3) the influence of topography and fracture is not considered in this numerical simulation; (4) the orientations of σ_H and σ_h are considered horizontal, and the orientation of σ_v is vertical.

3.1. Geological Conceptual Model. The prototype of the deep-buried-curved tunnel is a typical two-lane high-speed passenger line widely used in China now (Figure 3), with speeds of 300 km/h and 350 km/h according to the code for design of high-speed railway [59]. The span and the arch height of the curved tunnel are 13.3 m and 10.53 m, respectively. The dimension of the model is $x \times y \times z = 140\,\text{m} \times 140\,\text{m} \times 140\,\text{m}$. Statistics show that rockburst always occurs with the buried depth over 700 m in tunnel construction [60]; therefore, the model is considered at a depth of 700 m underground.

3.2. Numerical Modeling

3.2.1. Meshed Model and Boundary Condition. Ten numerical models were established to actualize transformation of φ from 0° to 90°. For the sake of enhancing the accuracy of the result, the models are divided into core part meshed same in each model and the marginal part meshed differently with same number of nodes and elements generally. Different loading orientations of in situ stress could be realized by marginal part grid. The interface between tunnel end and marginal part belongs to free surface. It is generally considered that stress redistributed of surrounding rock is caused by underground chamber excavation within 6 times radius of the hole [61]. The tunnel model is located at the core part of the model rather than through the whole model.

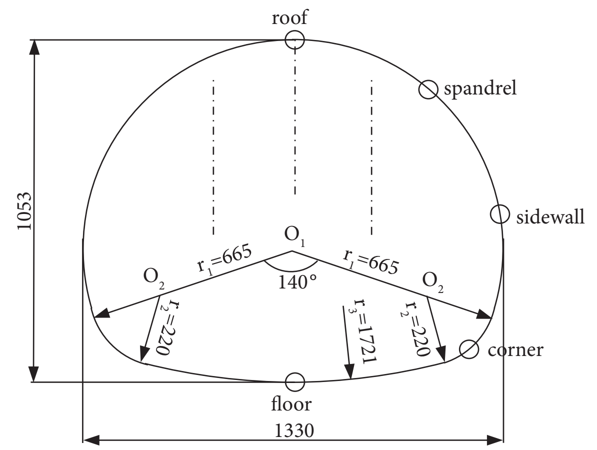

Figure 3: Railway tunnel for a two-lane high-speed passenger line with speeds of 300 km/h and 350 km/h (unit: mm).

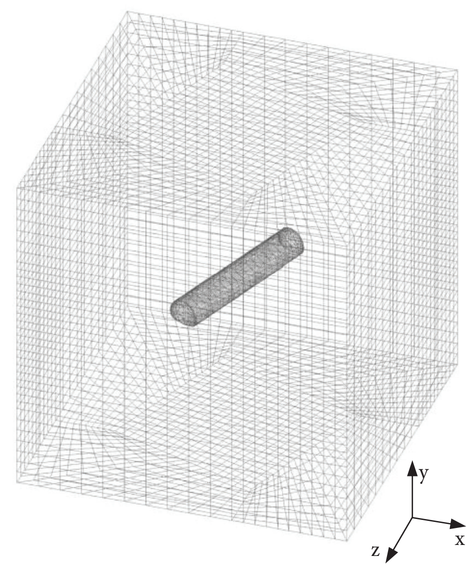

Figure 4: Meshed model ($\varphi = 20^\circ$).

Tunnel ends belong to the junction site of the core part and the marginal part. The distance from tunnel ends to the tunnel middle cross-section far exceeds six times of tunnel radius. Therefore, the effect of the tunnel ends on the middle cross-section of the selected analysis data is basically ignored.

Each model is meshed by three-dimensional eight-node solid element type (Figure 4). Since horizontal principal stress and vertical stress changed less by gradient in model range for the deep-buried tunnel, constants force of σ_H, σ_h, and σ_v are loaded to model. The boundary conditions for stress and displacement are applied to the model demonstrated in Figures 5 and 6. σ_v is applied to models with a magnitude of 19.04 MPa, which is calculated by overburden rock. σ_H and σ_h are assigned by various K_H to simulate different in situ stress states; thus, the ratio K_h of σ_h and σ_v is determined. According to the in situ stress data of Qinghai-Tibet Plateau and its adjacent region with strong tectonic action, $\sigma_H/\sigma_h = 1.53$ is utilized in the model to loading [47, 48].

3.2.2. Mechanical Parameter. Considering the occurrence of rockburst in actual situation [62], the mechanical parameters of surrounding rock mass of grade II are selected as given Table 1, based on the prototype of surrounding rock mass of grade II in TB 10621-2009 [59].

3.2.3. Simulation Conditions. To analyze the coupling effect of the orientation of σ_H and K_H, 50 different calculation conditions are presented to numerical simulation. Depending on the analyze on part 2, different in situ stress states in Qinghai-Tibet Plateau and its adjacent region were simulated. The associations of φ and K_H are given in Table 2.

4. Stress Redistribution of Surrounding Rock Mass in 50 Simulation Conditions

The stress redistribution caused by deep-buried tunnels excavation leading stress concentration may trigger

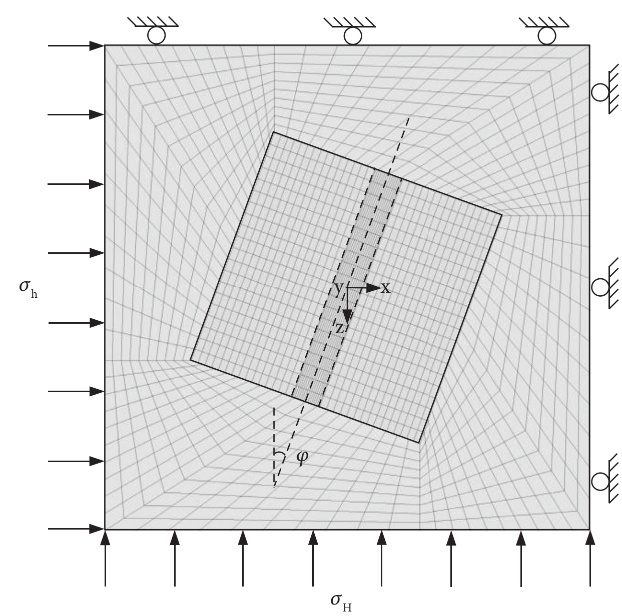

Figure 5: *x-z* section view of the meshed model with specific boundaries and loading conditions ($\varphi = 20^\circ$).

rockburst. Due to the failure of surrounding rock mass developing from the boundary of the tunnel to the interior rock mass along radius direction [61], σ_θ in surrounding rock mass of the deep-buried-curved tunnel from numerical simulation based on in situ stress state of Qinghai-Tibet Plateau and its adjacent region is analyzed in this study.

As Figure 7 shows, the positions of stress concentration are deeply related to K_H and φ for the deep-buried-curved tunnel. The main features are described as follows:

$K_H \geq 2$: the compressive σ_θ concentrated position in the surrounding rock mass of the tunnel is not obvious when $\varphi \leq 20^\circ$. With the increase of φ, σ_θ gradually concentrates in surrounding rock mass at roof, floor,

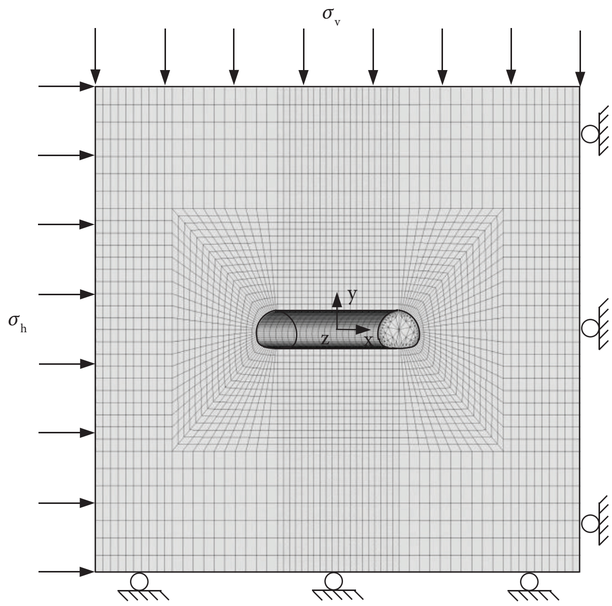

Figure 6: x-y section view of the meshed model at middle with specific boundaries and loading conditions ($\varphi = 20^{\circ}$).

Table 1: Mechanical parameters of surrounding rock of grade II.

Surrounding rock of grade II	Density (ρ) (g/m^3)	Elastic modulus (GPa)	Poisson's ratio (μ)
Prototype	>2.65	16–33	0.2–0.25
Model	2.72	16	0.25

Table 2: Cases for simulation conditions.

K_H		φ Angle between the maximum horizontal principal stress orientation and tunnel axis (°)									
		0°	10°	20°	30°	40°	50°	60°	70°	80°	90°
Lateral pressure coefficient	0.5	√	√	√	√	√	√	√	√	√	√
	1	√	√	√	√	√	√	√	√	√	√
	1.5	√	√	√	√	√	√	√	√	√	√
	2	√	√	√	√	√	√	√	√	√	√
	2.5	√	√	√	√	√	√	√	√	√	√

and corner, while σ_θ concentration at sidewall diminishes.

$K_H = 1.5$: while $\varphi \leq 20^{\circ}$, σ_θ concentration emerges mainly in the surrounding rock mass at corner and sidewall. σ_θ concentration in surrounding rock mass at sidewall gradually decreases when φ increases. Meanwhile, σ_θ at roof and floor increases, forming the compressive σ_θ concentration.

$K_H = 1$: with the increase of φ, the compressive σ_θ concentration in surrounding rock mass appears from sidewall to corner to spandrel to roof gradually.

$K_H = 0.5$: the compressive σ_θ concentration in surrounding rock mass appears at sidewall, which is slightly impacted by the in situ stress orientation under weak level horizontal tectonic stress. In addition, σ_θ at roof and floor is subjected to tensile stress while $\varphi \leq 40^{\circ}$, especially at floor.

Comparing the values of σ_θ at the key positions of the deep-buried-curved tunnel in different simulation conditions, it can be demonstrated that the compressive σ_θ at roof is obviously larger than that at bottom, and the compressive σ_θ at corner is greater than that at spandrel due to the asymmetry in shape of the tunnel in horizontal and in situ stress states of Qinghai-Tibet Plateau and its adjacent region.

5. The Influence of In Situ Stress State on the Tunnel Stability

Rockburst plays a pivotal role in the failure of the tunnel under the condition of high in situ stress. Indexes correlating

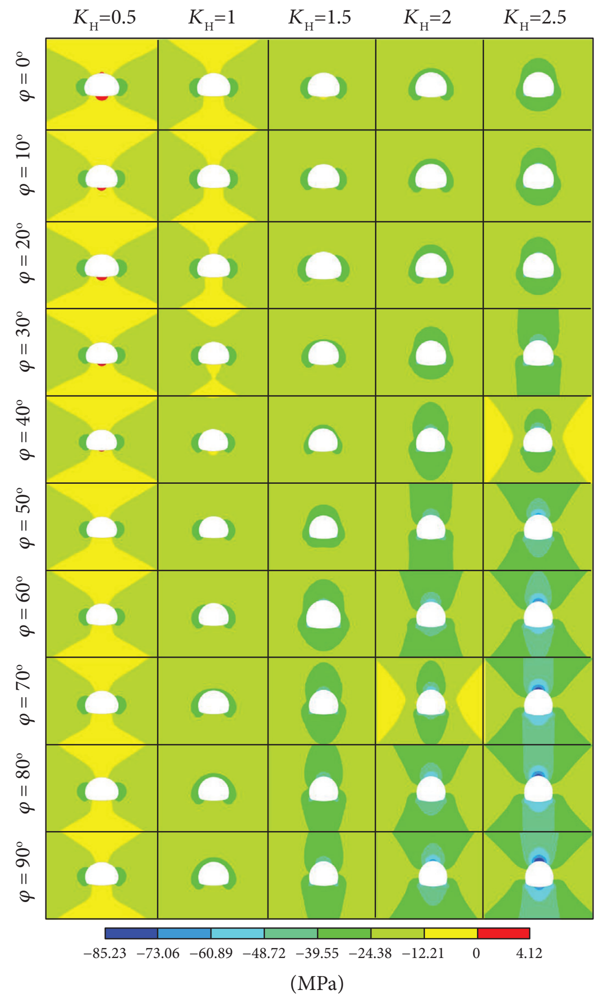

Figure 7: The distribution of tangential stress σ_θ in surrounding rock of the tunnel under various simulation conditions (the tensile stress is positive and the compressive stress is negative).

to the maximum tangential stress on the boundary of the tunnel $\sigma_{\theta\max}$ and uniaxial compressive strength σ_c are widely used as empirical criteria in the potential of strain rockburst [63–68].

To analyze the feature of σ_θ in the deep-buried-curved tunnel, five key positions located at roof, floor, spandrel, corner, and sidewall around the boundary of the tunnel were chosen to carry out σ_θ under various in situ stress states in the numerical simulation, respectively, as shown in Figure 3. From theory and practice, the key positions are the most prone position to fracture [41, 61, 69, 70]. The rockburst potential of the five key positions analyzed under σ_c is 60 MPa (this is done for convenience, but it is not a limitation of the result).

5.1. Effect of φ on Tunnel Stability. It is revealed from Figure 8 that under the identical K_H condition, σ_θ increases with the growth of φ at roof, floor, spandrel, and corner of the tunnel, which is disadvantageous for the safety of the tunnel; simultaneously, the risk of rockburst enhances under the same condition of σ_c. In this regard, σ_θ at sidewall diminishes with the increase of φ in identical K_H condition, making the potential for rockburst reduce with the same σ_c, which avails to tunnel stability. The relationship is observed between the key positions σ_θ and φ with approximately trigonometric function in constant K_H.

When $30° < \varphi < 60°$, it is noticed that the transformation of φ has a significant impact on σ_θ at the five key positions. Also, the transformation of φ exerts notable influence on the potential of rockburst in constant σ_c and the tunnel stability. Particularly, the effect on σ_θ is the most pronounced while φ is about 45° due to the slope of the curve is the sharpest. With $\varphi > 45°$, as the increase of φ, the effect on σ_θ at key positions becomes slighter. Moreover, the influence on the potential of rockburst in constant σ_c as well as tunnel stability decreases gradually by the change of φ. With $\varphi < 45°$, the effect on σ_θ at the key positions becomes greater as φ increases. The influence of potential of rockburst in constant σ_c and tunnel stability increases gradually with the variation of φ. The effect on σ_θ and tunnel stability is marginally affected by altering on φ, while σ_H is parallel and vertical to the tunnel axis.

5.2. Effect of K_H on Tunnel Stability. It is indicated from Figure 9 that σ_θ increases with the enhancement of K_H under the identical φ at roof, floor, spandrel, and corner of the tunnel periphery. The corresponding rockburst potential increases sharply with constant σ_c and tunnel stability seriously reduced. However, for the sidewall of the tunnel, the increase of K_H results in σ_θ reduced and rockburst potential diminished in the equivalent σ_c, and thus, the stability of tunnel enhanced. The relationship is observed between the key positions σ_θ and K_H with approximately linear function in constant φ.

The effect of K_H variation is discrepant under various φ at different key positions. It can be observed that with the increase in φ, the influence of K_H transformation on σ_θ is significantly enhanced, which means that the change of K_H at a large φ has greater influence than that at a small φ. The effect of K_H variation on potential of rockburst in constant σ_c and tunnel stability is the slightest when σ_H is parallel with the tunnel axis. On the contrary, the effect of K_H variation on potential of rockburst in constant σ_c and tunnel stability is the most prominent when σ_H is perpendicular to the tunnel axis.

6. Multivariate Regression Analysis of σ_θ

6.1. Analytical Solution of the Stress in Circular Cross-Section of Deep-Buried Tunnel. This study presents an analytical solution to calculate the stresses in unsupported deep-buried tunnels in various in situ stress states. Assumptions of analytical solution are the same as numerical simulation. While σ_H is not parallel with tunnel axis, the in situ stress tensor can be rotated to coordinate $x'yz'$, so that z' is parallel with the tunnel axial direction for the convenience to calculate (Figure 10). The initial stress state of the tunnel based on the $x'yz'$ coordinate system derived from the stress transform can be expressed as

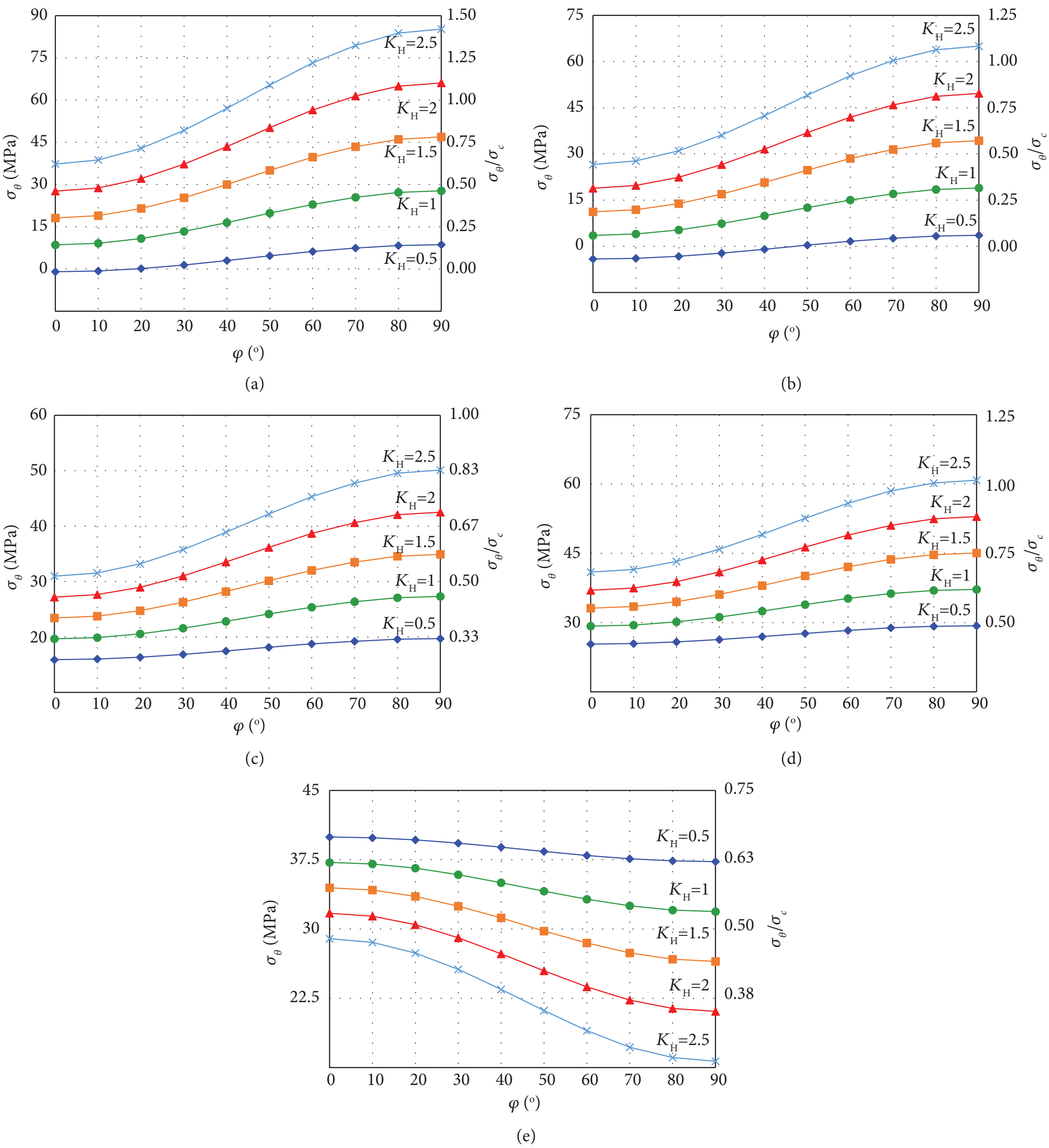

Figure 8: The tangential stress σ_θ and $\sigma_\theta/\ \sigma_c$ curves at the key positions of the tunnel under various angles φ between the maximum horizontal principal stress orientation and tunnel axis. (a) Roof. (b) Floor. (c) Spandrel. (d) Corner. (e) Sidewall.

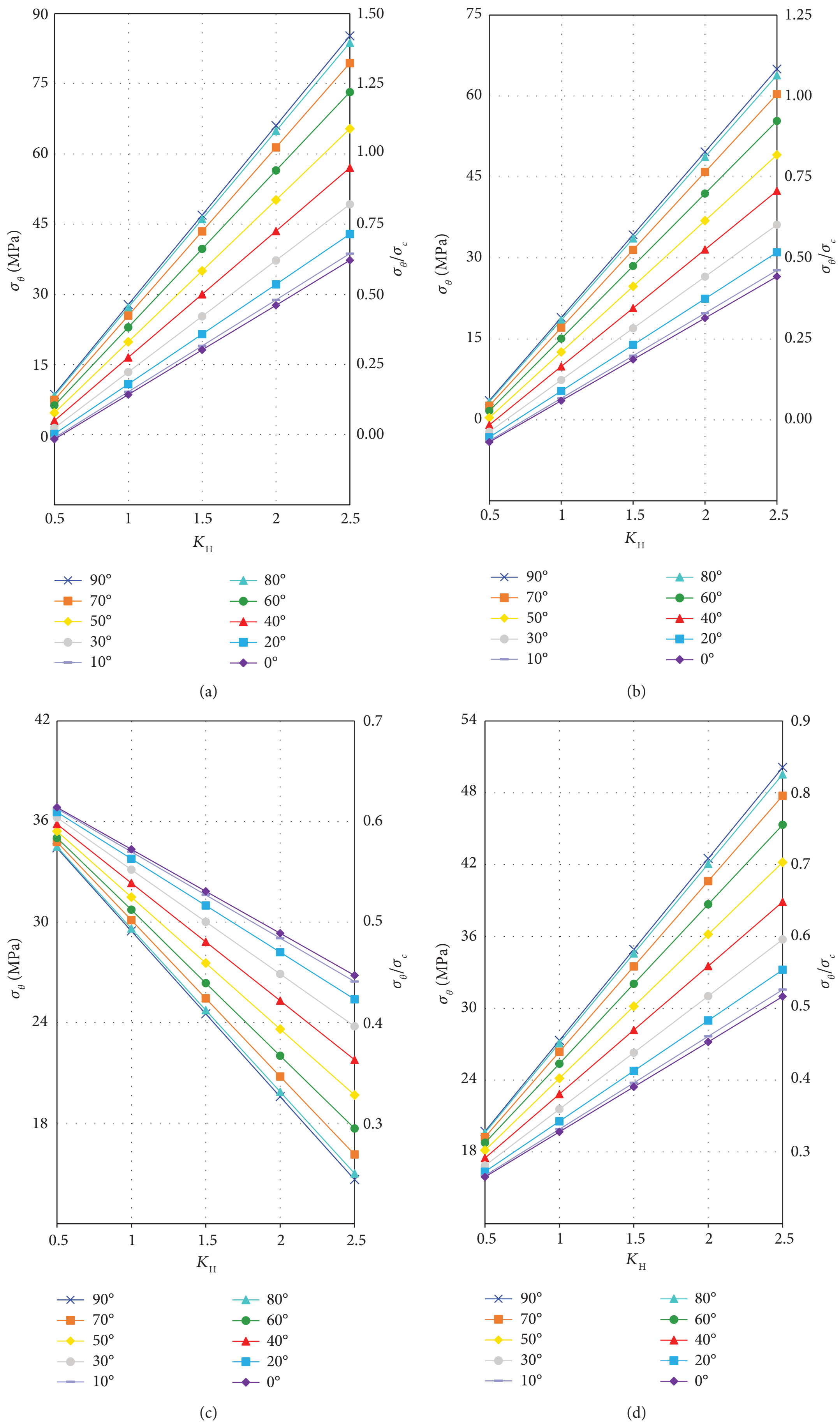

Figure 9: Continued.

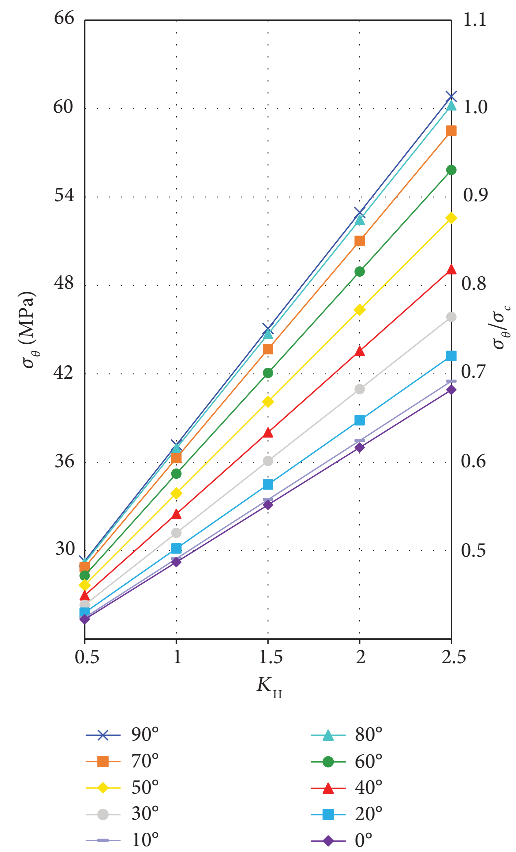

(e)

Figure 9: The tangential stress σ_θ and $\sigma_\theta/\ \sigma_c$ curves at the key positions of the tunnel under various lateral pressure coefficient K_H. (a) Roof. (b) Floor. (c) Sidewall. (d) Spandrel. (e) Corner.

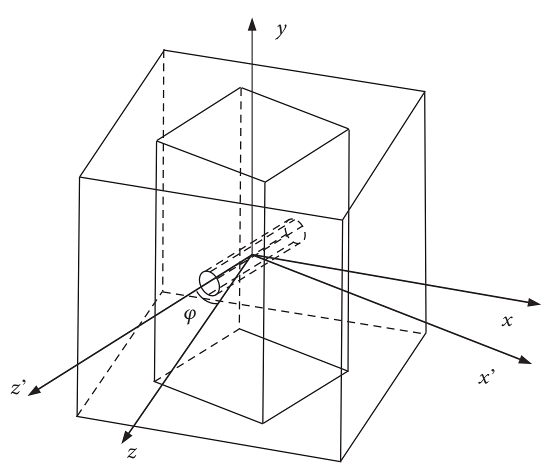

Figure 10: Schematic diagram of the rotation of in situ stress tensor.

$$\begin{cases} \sigma_{x'} = \sigma_H \sin^2\varphi + \sigma_h \cos^2\varphi, \\ \sigma_{z'} = \sigma_H \cos^2\varphi + \sigma_h \sin^2\varphi, \\ \sigma_y = \sigma_v, \\ \tau_{x'z'} = (\sigma_H + \sigma_h)\sin\varphi\cos\varphi, \\ \tau_{x'y} = 0, \\ \tau_{yz'} = 0, \end{cases} \tag{1}$$

where $\sigma_{x'}$ are the initial horizontal stress components vertical to tunnel axis; $\sigma_{z'}$ are the initial horizontal stress components parallel to tunnel axis; σ_y are the initial vertical stress components; and $\tau_{x'z'}, \tau_{x'y}, \tau_{yz'}$ are the initial shear stress components in the x'-z' plane, x'-y plane, and y-z' plane, respectively.

Figures 11 and 12 show the x'-y section and the x'-z' section view of stress state when z' is parallel to the tunnel axis ($\varphi = 0°$). The redistribution stress of horizontal circular tunnels deep-buried in elastic rock mass can be solved by Kirsch [49] based on two-dimensional plain strain conditions. For liner elastic, the initial axial normal stress has no effect on the radial and the tangential stresses on an infinitely long tunnel. Redistribution of stresses in the circular tunnel in three-dimensional stress field can be obtained from the combination of Kirsch [49] and stress redistribution of the circular tunnel under initial shear stress [32]. Because of the superposition principle, it can be expressed as

$$\begin{cases} \sigma_\theta = \dfrac{\sigma_{x'} + \sigma_v}{2}\left[1 + \left(\dfrac{r_0}{r}\right)^2\right] - \dfrac{\sigma_{x'} - \sigma_v}{2}\left[1 + 3\left(\dfrac{r_0}{r}\right)^4\right]\cos 2\theta, \\ \sigma_r = \dfrac{\sigma_{x'} + \sigma_v}{2}\left[1 - \left(\dfrac{r_0}{r}\right)^2\right] + \dfrac{\sigma_{x'} - \sigma_v}{2}\left[1 + 3\left(\dfrac{r_0}{r}\right)^4 - 4\left(\dfrac{r_0}{r}\right)^2\right]\cos 2\theta, \\ \tau_{r\theta} = -\dfrac{\sigma_{x'} - \sigma_v}{2}\left[1 + 2\left(\dfrac{r_0}{r}\right)^2 - 3\left(\dfrac{r_0}{r}\right)^4\right]\sin 2\theta, \\ \tau_{z'\theta} = -\left[1 + \left(\dfrac{r_0}{r}\right)^2\right]\tau_{x'z'}\sin\theta, \\ \tau_{z'r} = \left[1 - \left(\dfrac{r_0}{r}\right)^2\right]\tau_{x'z'}\cos\theta, \end{cases} \tag{2}$$

where r_0 is the radius of the tunnel; r, θ represent the radius vector and polar angle in the $r\theta z'$ cylindrical coordinate; and $\tau_{r\theta}, \tau_{z'\theta}, \tau_{z'r}$ are shear stresses in the $r\theta z'$ cylindrical coordinate.

For $r = r_0$, the redistribution stress is equivalent to

$$\begin{cases} \sigma_\theta = \sigma_{x'} + \sigma_v - 2(\sigma_{x'} - \sigma_v)\cos 2\theta, \\ \sigma_r = 0, \\ \tau_{r\theta} = 0, \\ \tau_{z'\theta} = -2\tau_{x'z'}\sin\theta, \\ \tau_{z'r} = 0. \end{cases} \tag{3}$$

Substituting equation (1) with (3), the analytical solution for redistribution stress in various in situ stress states can be given as

$$\begin{cases} \sigma_\theta = \sigma_v\left\{K_H\left[\left(\dfrac{1}{2} - \cos 2\theta\right)\left(\dfrac{\sigma_h}{\sigma_H} - 1\right)\cos 2\varphi + \dfrac{1}{2} - \cos 2\theta\right] + K_h\left(\dfrac{1}{2} - \cos 2\theta\right) + 2\cos 2\theta + 1\right\}, \\ \tau_{z'\theta} = -2\sigma_v(K_H + K_h)\sin\varphi\cos\varphi\sin\theta. \end{cases} \tag{4}$$

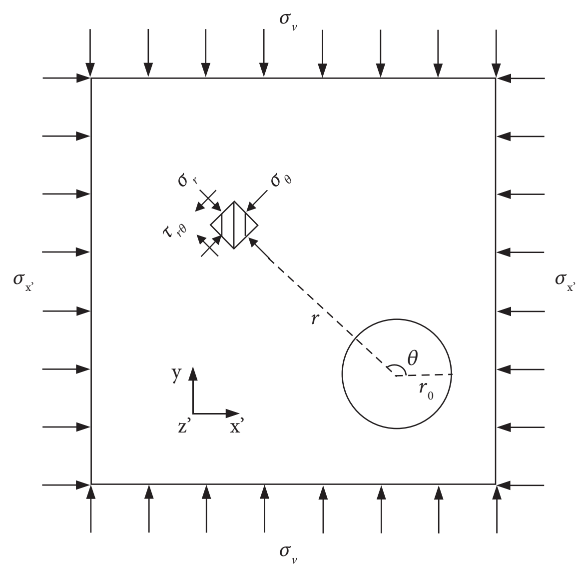

Figure 11: The x'-y section view of stress state ($\varphi = 0°$).

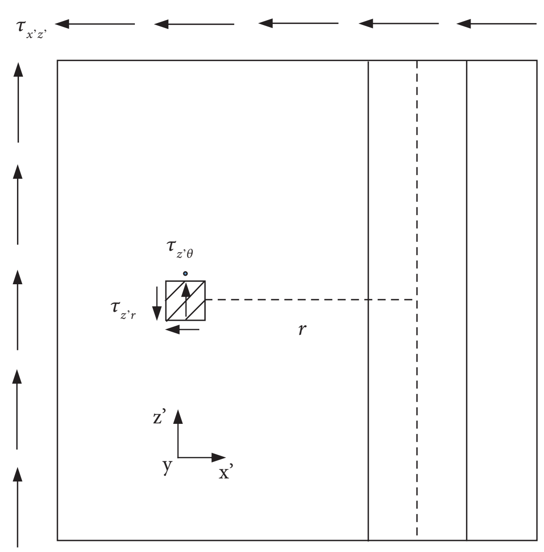

Figure 12: The x'-z' section view of stress state ($\varphi = 0°$).

6.2. Multivariate Regression Equation of σ_θ. The purpose of the multivariate regression analysis method is to construct relationships between σ_θ with φ, K_H at the key positions. Multivariate regression analysis develops the empirical models to introduce predictive equations which generated by results of stress redistribution in the key positions at deep-buried-curved tunnels from numerical simulation and data analysis in Qinghai-Tibet Plateau and its adjacent region. The form proposed from equation (4) can be applied to predict σ_θ in different key positions. The tunnel shape in the numerical model is made up of three arcs of different diameters based on TB 10621-2009 (Figure 3), and the theoretical formula is derived from an ideal circular tunnel. The form of predictive equations developed from theoretical formula. Multivariate regression analysis develops predictive equations, generated by results of stress redistribution from numerical simulation and data analysis in Qinghai-Tibet Plateau and its adjacent region. A summary of regression equations is given in Table 3. As given in Table 3, the adjust R^2 between predictive equations and stress redistribution data based on numerical simulation were all greater than 99%, which mean the predictive equation fitting the data from numerical simulation well. Hence, the effect of simplified shape of analysis is minimal, and the predictive equations reliably reflected relationships between σ_θ with φ, K_H at the key positions. On the other hand, predictive equation verified that the relationship between φ and σ_θ at key position is trigonometric function in constant K_H. Also, the relationship between K_H and σ_θ at the key positions is linear function in constant φ.

The validity of the overall equations can be approved using an F-test [71, 72]. The value of F is calculated by the analysis of variance (ANOVA) and is given in Table 4. As given in Table 4, the F-test, with very low probability value (Prob (F)), demonstrates a very high significance for the predictive equations and confirms the adequacy of predictive equations. Besides, as given in Table 3, very high adjusted R^2 values indicate that predictive equations are believable.

Therefore, for a deep-buried-curved tunnel in Qinghai-Tibet Plateau and its adjacent region with determined in situ stress state condition, the equations can be used easily to quantitatively calculate σ_θ. Combined with σ_c, the prediction of rockburst intensity evaluated by corresponding criteria and the potential location of high-risk area of rockburst are obtained without need of too much geo-stress background knowledge and heavy simulation. The response surfaces between σ_θ with φ and K_H at the key positions are shown in Figure 13, respectively. The predictive equations and response surfaces also represent a straightforward tool for quickly estimating the potential altering tendency of tunnel stability under different tunnel axis layout conditions and in situ stress state at tunnel design and planning stage in

Table 3: The predictive equations and their adjusted R^2 values at key positions.

Position	Predictive equation	Adjusted R^2 (%)
Roof	$\sigma_\theta = (-9.588\cos 2\varphi + 28.69) \times K_H - 10.53$	99.97
Floor	$\sigma_\theta = (-7.686\cos 2\varphi + 23.02) \times K_H - 11.79$	99.98
Spandrel	$\sigma_\theta = (-3.822\cos 2\varphi + 11.36) \times K_H + 12.12$	99.97
Corner	$\sigma_\theta = (-3.985\cos 2\varphi + 11.77) \times K_H + 21.43$	99.97
Sidewall	$\sigma_\theta = (2.433\cos 2\varphi - 7.455) \times K_H + 39.37$	99.99

The unit of σ_θ is MPa; the unit of φ is rad.

Table 4: ANOVA table for the models for assessing σ_θ of the different positions in various in situ stress states.

Position	Source	Sum of squares	DF	Mean square	F ratio	Probability (f)
Roof	K_H	20582.9	4	5145.72	146.69	0.00
	φ	5689.5	9	632.17	18.02	0.00
	Error	1262.9	36	35.08	—	—
	Total	27535.3	49	—	—	—
Floor	K_H	13242.3	4	3310.57	146.84	0.00
	φ	3655.8	9	406.2	18.02	0.00
	Error	811.6	36	22.54	—	—
	Total	17709.7	49	—	—	—
Corner	K_H	3460.39	4	865.099	142.55	0.00
	φ	982.5	9	109.167	17.99	0.00
	Error	218.48	36	6.069	—	—
	Total	4661.37	49	—	—	—
Spandrel	K_H	3227.38	4	806.844	144.12	0.00
	φ	903.46	9	100.385	17.93	0.00
	Error	201.54	36	5.598	—	—
	Total	4332.38	49	—	—	—
Sidewall	K_H	3227.38	4	806.844	144.12	0.00
	φ	903.46	9	100.385	17.93	0.00
	Error	201.54	36	5.598	—	—
	Total	4332.38	49	—	—	—

Qinghai-Tibet Plateau and its adjacent region. This will also serve to aid scientific evidences for rockburst risk prevention of tunnel construction.

7. Discussion

For the scientificity, practicality and availability of predictive equations for σ_θ at the key positions in the deep-buried-curved tunnel are based on Qinghai-Tibet Plateau and its adjacent region, and it is essential to verify the accuracy of rockburst intensity of predictive equations.

The value of $(\sigma_{\theta\max}/\sigma_c)$ as a significant criterion is extensively applied, while many debates for the valuation of the criterion still exist [65, 67, 73, 74]. Russenes criterion was utilized in this study (Table 5).

Based on the in situ measured stress data, we calculated σ_θ to obtain rockburst intensity compared with other rockburst potential assess methods (numerical simulation, physical simulation, and empirical criteria) and actual construction, as given in Table 6.

It is revealed that the multiple regression constructed by numerical results are in good agreement with rockburst intensity in actual construction as well as prediction by various methods. The result indicates that the simulated prediction equations rockburst could well reflect the rockburst feature in various in situ stress states and possess scientific merit in and wide practical value in the deep-buried tunnel in Qinghai-Tibet Plateau and its adjacent region.

It should be mentioned that the stability of the tunnel is also related to other factors apart from K_H and φ, such as preexisting joints, active fault, topography, nonuniformity, and nonelasticity of rock mass.

The presence of joints, which causes asymmetrical loading and local instabilities when underground tunnel excavation, has close relationship to failures in surrounding rock. Preexisting joints in rock mass affect the mechanical behavior and weaken the strength of surrounding rock mass in tunnel boundary, reflected in the effect of frequency, orientation of joint, and shear strength along the critical joint set [89, 90].

Active faults are potential sources of earthquake. The coseismic dislocation of active faults could destroy most structures that span faults, posing a threat to the stability of the tunnel in the tectonic active area. As for railways are generally linear projects, it is important for railways to avoid crossing active faults as possible [91–93]. Moreover, active faults may change stress between the void and the discontinuity and alter the orientation of local stress [19, 26].

Furthermore, the orientations of σ_H and σ_h always have dips, not absolutely horizontal, and the orientation of σ_v also has a dip, not absolutely vertical. Based on the research

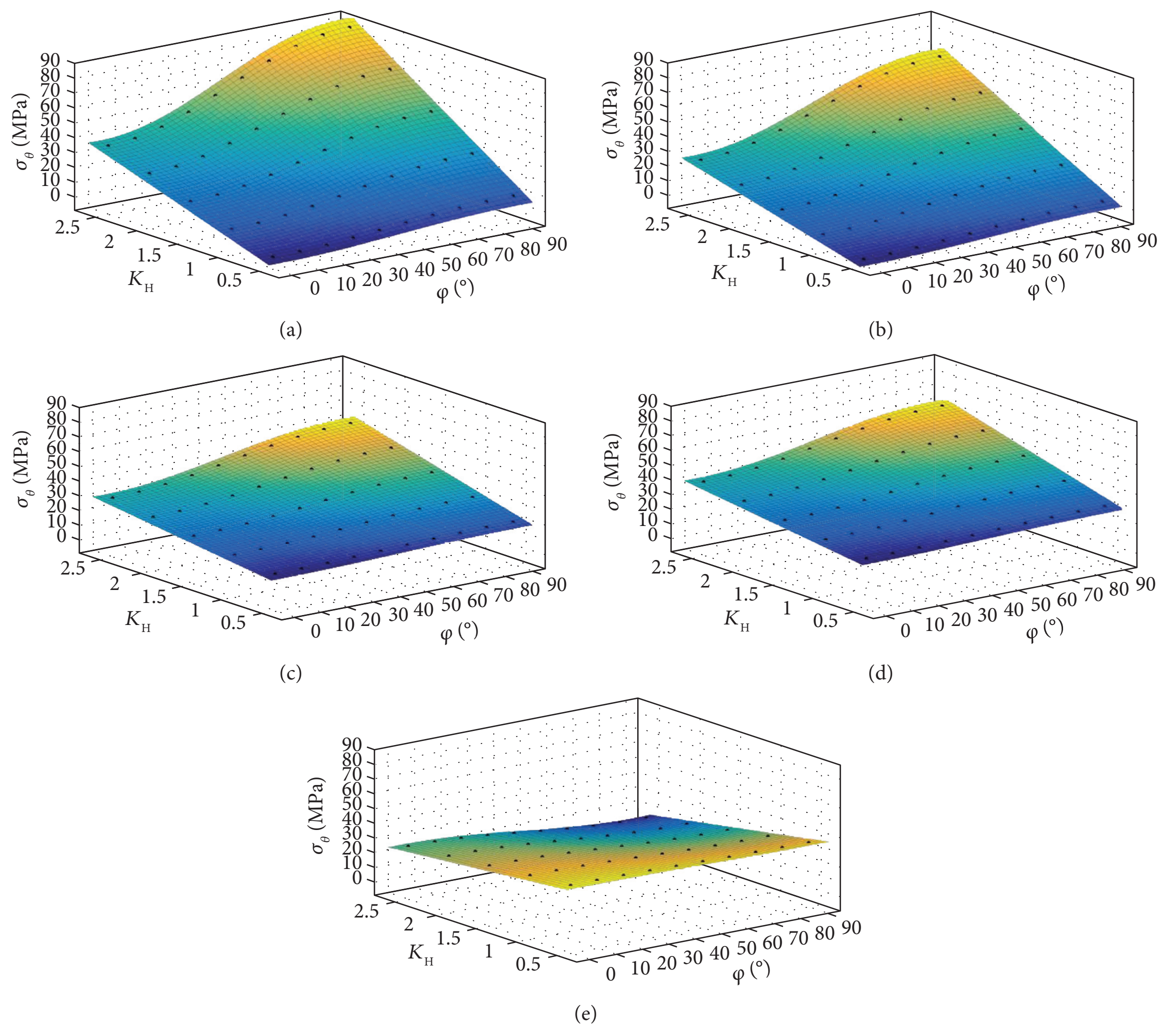

Figure 13: Response surface of the tunnel in key positions. (a) Roof. (b) Floor. (c) Spandrel. (d) Corner. (e) Sidewall.

Table 5: Rockburst criterion from Russenes.

Index	No rockburst	Weak rockburst	Moderate rockburst	Severe rockburst
$\sigma_{\theta\max}/\sigma_c$	<0.2	0.2-0.3	0.3–0.55	≥0.55

Table 6: Comparison of rockburst intensity between predictive equations and actual construction at typical deep-buried tunnels.

	Deep-buried tunnel	The maximum depth (m)	In situ stress measurement									Rockburst intensity		
			Lithology	Text depth (m)	σ_H (MPa)	σ_v (MPa)	K_H	σ_c (MPa)	φ (°)	$\sigma_{\theta\max}$ (MPa) (position)	σ_θ/σ_c	Predictive equations	Other assess methods	Actual construction
1	Chainage 09+706 in the Neelum-Jhelum Hydroelectric Project, Pakistan [18]	1860	Sandstone	1550	Unclear	Unclear	1.25	86	90	41.19 (roof)	0.77	Severe	Severe	Severe
2	Guigala Expressway tunnel, China [75]	1200	Granite	560	21.78	14.84	1.47	75.4	89	45.64 (roof)	0.6	Severe	Severe	Unclear
3	Dangjinshan railway tunnel, China [76]	764	Mica, quartz, schist	551	28.56	14.64	1.95	87	21	38.61 (corner)	0.50	Moderate	Moderate	Unclear
4	Bayu railway tunnel, China [44]	2073	Granite	583	17.72	15.13	1.17	151.9	87	39.85 (corner)	0.42	Moderate	Moderate	Yes
5	Gaoligong mountain railway tunnel, China [77, 78]	1600	Granite	699	28.68	18.87	1.52	70.7–125.4	15	34.07 (corner)	0.28–0.48	Weak-moderate	Yes	Weak-moderate
6	7# laboratory of Jinping II Hydropower Station, China [79, 60]	2525	Marble	2400	67.32	69.2	0.97	99–114	45	51.67 (corner and sidewall)	0.23–0.33	Weak-moderate	Unclear	Weak-moderate, spalling
7	Zheduoshan railway tunnel, China [15]	1124	Quartz and siltstone	248	17.44	6.55	2.66	62.2–140.6	30	53.12 (roof)	0.37–0.85	Moderate-severe	Moderate-severe	Unclear
8	Erlang Mountain highway tunnel, China [16, 61]	760	Siltstone	750	35.3	8.1	4.36	139.9	20	82.48 (roof)	0.59	Severe	Unclear	Severe
9	Muzhailing railway tunnel, China [62]	600	Sandstone	330	26.22	8.95	2.93	94.5–98.5	3.5	45.64 (roof)	0.46–0.48	Moderate	Moderate	Yes
10	Micang Mountain highway tunnel, China [45]	>1000	Granite	600	28.43	11.94	1.18	102.7	86	81.52 (roof)	0.78	Severe	Severe	Yes
11	Ping'an tunnel, China [83]	Unclear	Limestone	1350–1430	31.52	15.17	2.08	28.7–76.6	6	37.79 (corner)	0.49–1.31	Moderate-severe	Moderate-severe	Moderate-severe
12	Qinling railway tunnel, China [84, 85]	1600	Granite	560	19.7	14.5	1.35	95–130	31	34.88 (corner)	0.27–0.37	Weak-moderate	Yes	Weak-moderate
13	Xinbaiyanzhai railway tunnel, China [86]	Unclear	Syenite	444	23.44	13.45	1.74	105.9–169.7	15	35.95 (corner)	0.21–0.33	Weak-moderate	Yes	Spalling
14	Baziling railway tunnel, China [87]	695	Limestone	546	14.95	14.46	1.02	64.6	51	57.04 (corner)	0.53	Moderate	Moderate	Unclear
15	−205 m level of Zhazixi Antimony Mine, China [88]	605	Quartz and sandstone	605	19.61	8	2.05	65.2	22	39.20 (corner)	0.60	Severe	Unclear	Severe

Note: "yes" means rockburst occured but intensity unknown.

results from Feng et al. [94], the assumptions of the orientations of the three principal stresses can be accepted in Qinghai-Tibet Plateau and its adjacent region.

Here, due to the complicated geological and structure of rock mass, the effect of above factors is not taken into consideration in this research. However, the predictive equations are proved effective through verification in a set of actual construction tunnels. The impact of above conditions on σ_θ and stability of the tunnel is needed to explore to improve the understanding of this study in further work.

8. Conclusion

This study analyzed the coupling effect of the angle φ between the maximum horizontal principal stress orientation and tunnel axis and lateral pressure coefficient K_H on the stability of the deep-buried-curved tunnel under the in situ stress state of Qinghai-Tibet Plateau and its adjacent region. The conclusions are as follows:

(1) Stress redistribution of surrounding rock mass in 50 simulation conditions is systematically analyzed. When $\varphi \leq 20^\circ$, the positions of σ_θ concentration are related to the lateral pressure coefficient. With the increase of φ, σ_θ concentration at the sidewall of the tunnel diminishes gradually, while σ_θ at roof, floor, and corner of the tunnel forms concentration. Whereas, under weak horizontal tectonic stress action, the positions of stress concentration are slightly impacted by the stress orientation.

(2) With the increase of φ, σ_θ increases at roof, floor, spandrel, and corner of the tunnel periphery under the identical K_H; the corresponding σ_θ decreases at sidewall. When $30^\circ < \varphi < 60^\circ$, the transformation of φ has a significant impact on σ_θ and tunnel stability. Especially when φ is about 45°, σ_θ and the stability of the tunnel are obviously affected.

(3) σ_θ increases with the improvement of K_H under the identical φ at roof, floor, spandrel, and corner of the tunnel periphery, whereas σ_θ reduces at sidewall of the tunnel. With the increase in φ, the influence of K_H transformation on σ_θ and tunnel stability is significantly enhanced. The influence of tunnel stability is the slightest with $\varphi = 0^\circ$. On the country, the influence is maximum when $\varphi = 90^\circ$.

(4) Predictive equations and response surfaces for σ_θ at the key positions (roof, floor, spandrel, corner, and sidewall) of the tunnel based on multiple regression modeling are proposed and verified by a set of typical tunnels. The equations can be employed easily to quantitatively calculate σ_θ for a deep-buried-curved tunnel in determined in situ stress state condition to rapidly estimate rockburst intensity and evaluate the potential altering tendency of tunnel stability under different tunnel axes and in situ stress states at the planning and designing stage of the deep tunnel.

Data Availability

The datasets used or analyzed during the current study are available from the corresponding author upon request.

Conflicts of Interest

The authors declare that there are no conflicts of interest.

Acknowledgments

The authors gratefully acknowledge the financial support from China Geological Survey (DD20160267 and DD20190317) and the National Natural Science Foundation of China (DD41702341).

References

[1] T. Solak, “Ground behavior evaluation for tunnels in blocky rock masses,” *Tunnelling and Underground Space Technology*, vol. 24, no. 3, pp. 323–330, 2009.

[2] A. Mazaira and P. Konicek, “Intense rockburst impacts in deep underground construction and their prevention,” *Canadian Geotechnical Journal*, vol. 52, no. 10, pp. 1426–1439, 2015.

[3] W. Zhang, X. T. Feng, X. Yaxun et al., “A rockburst intensity criterion based on the geological strength index, experiences learned from a deep tunnel,” *Bulletin of Engineering Geology and the Environment*, vol. 79, pp. 3585–3603, 2020.

[4] J. Zhou, X. B. Li, and H. S. Mitri, “Evaluation method of rockburst: state-of-the-art literature review,” *Tunnelling and Underground Space Technology*, vol. 81, pp. 632–659, 2018.

[5] P. Molnar, P. England, and J. Martinod, “Mantle dynamics, uplift of the Tibetan plateau, and the Indian monsoon,” *Reviews of Geophysics*, vol. 31, no. 4, pp. 357–396, 1993.

[6] S. Turner, C. Hawkesworth, J. Q. Liu, N. Rogers, S. Kelley, and P. V. Calsteren, “Timing of Tibetan uplift constrained by analysis of volcanic rocks,” *Nature*, vol. 364, no. 6432, pp. 50–54, 1993.

[7] Z. Chen, C. He, W. Yang, W. Guo, Z. Li, and G. Xu, “Impacts of geological conditions on instability causes and mechanical behavior of large-scale tunnels: a case study from the Sichuan-Tibet highway, China,” *Bulletin of Engineering Geology and the Environment*, vol. 79, no. 7, pp. 3667–3688, 2020.

[8] M. A. Murphy, A. Yin, T. M. Harrison et al., “Did the Indo-Asian collision alone create the Tibetan plateau,” *Geology*, vol. 25, pp. 719–722, 1997.

[9] B. S. Qi, D. G. Hu, X. X. Yang et al., “Apatite fission track evidence for the cretaceous-cenozoic cooling history of the Qilian Shan (NW-China) and for stepwise northeastward growth of the northeastern Tibetan plateau since early Eocene,” *Journal of Asian Earth Sciences*, vol. 124, pp. 28–41, 2016.

[10] P. Tapponnier, Z. Xu, F. Roger et al., “Oblique stepwise rise and growth of the Tibet plateau,” *Science*, vol. 294, no. 23, pp. 1671–1677, 2001.

[11] C. Wang, X. Zhao, Z. Liu et al., "Constrains on the early uplift history of the Tibetan plateau," *PNAS*, vol. 105, no. 13, pp. 4987–4992, 2008.

[12] A. Yin and T. M. Harrison, "Geolegic evolution of the Himalayan-Tibetan orogeny," *Annual Review of Earth & Planetary Sciences*, vol. 28, pp. 211–280, 2000.

[13] Q. A. Jiang, X. T. Feng, T. B. Xiang, and G. S. Su, "Rockburst characteristics and numerical simulation based on a new energy index: a case study of a tunnel at 2,500 m depth," *Bulletin of Engineering Geology and the Environment*, vol. 69, no. 3, pp. 381–388, 2010.

[14] S. J. Li, X. T. Feng, Z. H. Li, B. R. Chen, C. Q. Zhang, and H. Zhou, "In situ monitoring of rockburst nucleation and evolution in the deeply buried tunnels of Jinping II hydropower station," *Engineering Geology*, vol. 137, pp. 85–96, 2012.

[15] D. Wang, T. B. Li, L. W. Jiang, Z. H. Lin, and T. Feng, "Analysis of the stress characteristics and rock burst of ultra deep buried tunnel in Sichuan-Tibet railway," *Journal of Railway Engineering Society*, vol. 4, pp. 46–50, 2017, in Chinese.

[16] L. S. Xu, "Research of rockburst character and prevention measure in Erlang mountain highway tunnel," *China Civil Engineering Journal*, vol. 37, no. 1, pp. 61–64, 2004, in Chinese.

[17] C. Cao, C. Shi, M. Lei, W. Yang, and J. Liu, "Squeezing failure of tunnels: a case study," *Tunnelling and Underground Space Technology*, vol. 77, no. 7, pp. 188–203, 2018.

[18] A. M. Naji, M. Z. Emad, H. Rehman, and H. Yoo, "Geological and geomechanical heterogeneity in deep hydropower tunnels: a rock burst failure case study," *Tunnelling and Underground Space Technology*, vol. 84, pp. 507–521, 2019.

[19] A. M. Naji, H. Rehman, M. Z. Emad, and H. Yoo, "Impact of shear zone on rockburst in the deep Neelum-Jehlum hydropower tunnel: a numerical modeling approach," *Energies*, vol. 11, no. 8, p. 1935, 2018.

[20] Z. B. Qiao, "Study on rockburst intensity prediction based on the characteristics of in-situ stress field in deep tunnel at Sichuan-Tibet railway," *Railway Standard Design*, vol. 65, no. 2, pp. 89–103, 2021, in Chinese.

[21] Y. Zhu, *The Sichuan-Tibet Railway Construction Challenges and Countermeasures*, China Communications Press, Beijing, China, 2017, in Chinese.

[22] J. N. Franzius, D. M. Potts, and J. B. Burland, "The influence of soil anisotropy and K-0 on ground surface movements resulting from tunnel excavation," *Geotechnique*, vol. 55, no. 3, pp. 189–199, 2005.

[23] C. D. Martin, P. K. Kaiser, and R. Christiansson, "Stress, instability and design of underground excavations," *International Journal of Rock Mechanics and Mining Sciences*, vol. 40, no. 7-8, pp. 1027–1047, 2003.

[24] J. B. Martino and N. A. Chandler, "Excavation-induced damage studies at the underground research laboratory," *International Journal of Rock Mechanics and Mining Sciences*, vol. 41, no. 8, pp. 1413–1426, 2004.

[25] C. Tan, R. Wang, Y. Sun et al., "Numerical modelling estimation of the "tectonic stress plane" (TSP) beneath topography with quasi-U-shaped valleys," *International Journal of Rock Mechanics and Mining Sciences*, vol. 41, no. 2, pp. 303–310, 2004.

[26] V. A. Uskov, A. A. Eremenko, T. P. Darbinyan, and V. P. Marysyuk, "Geodynamic hazard assessment for tectonic structures in underground mining of north ore bodies in the oktyabrsky deposit," *Journal of Mining Science*, vol. 55, no. 1, pp. 77–87, 2019.

[27] E. Eberhardt, "Numerical modelling of three-dimension stress rotation ahead of an advancing tunnel face," *International Journal of Rock Mechanics and Mining Sciences*, vol. 38, no. 4, pp. 499–518, 2001.

[28] H. Konietzky, L. T. Kamp, H. Hammer, and S. Niedermeyer, "Numerical modelling of in situ stress conditions as an aid in route selection for rail tunnels in complex geological formations in south Germany," *Computers and Geotechnics*, vol. 28, no. 6-7, pp. 495–516, 2001.

[29] C. Q. Zhang, X. T. Feng, and H. Zhou, "Estimation of in situ stress along deep tunnels buried in complex geological conditions," *International Journal of Rock Mechanics and Mining Sciences*, vol. 52, pp. 139–162, 2012.

[30] R. E. Goodman, *Introduction to Rock Mechanics*, Wiley, New York, NY, USA, 1989.

[31] X. J. Li, L. G. Wang, and W. M. Yang, "A numerical study of underground cavern stability by geostress characteristics," *Shock and Vibration*, vol. 2016, Article ID 3768453, 13 pages, 2016.

[32] O. P. M. Vitali, T. B. Celestino, and A. Bobet, "Analytical solution for tunnels not aligned with geostatic principal stress directions," *Tunnelling and Underground Space Technology*, vol. 82, no. 12, pp. 394–405, 2018.

[33] L. Weng, X. Li, and M. Tao, "Influence of geostress orientation on fracture response of deep underground cavity subjected to dynamic loading," *Shock and Vibration*, vol. 2015, Article ID 575879, 9 pages, 2015.

[34] Z. Zhu, Y. Li, J. Xie, and B. Liu, "The effect of principal stress orientation on tunnel stability," *Tunnelling and Underground Space Technology*, vol. 49, pp. 279–286, 2015.

[35] Y. Luo, F. Q. Gong, D. Q. Liu, S. Y. Wang, and X. F. Si, "Experimental simulation analysis of the process and failure characteristics of spalling in D-shaped tunnels under true-triaxial loading conditions," *Tunnelling and Underground Space Technology*, vol. 90, pp. 42–61, 2019.

[36] Z. H. Li, W. C. Zhu, X. T. Feng, S. J. Li, H. Zhou, and B. R. Chen, "Effect of lateral pressure coefficients on damage and failure process of horseshoe-shaped tunnel," *Rock and Soil Mechanics*, vol. 31, no. S2, pp. 434–441, 2010, in Chinese.

[37] J. Tunsakul, P. Jongpradist, W. Kongkitkul, A. Wonglert, and S. Youwai, "Investigation of failure behavior of continuous rock mass around cavern under high internal pressure," *Tunnelling and Underground Space Technology*, vol. 82, no. 34, pp. 110–123, 2013.

[38] M. R. B. Golpasand, N. A. Do, D. Dias, and M. R. Nikudel, "Effect of the lateral earth pressure coefficient on settlements during mechanized tunneling," *Geomechanics and Engineering*, vol. 16, no. 6, pp. 643–654, 2018.

[39] X. B. Li and L. Weng, "Numerical investigation on fracturing behaviors of deep-buried opening under dynamic disturbance," *Tunnelling and Underground Space Technology*, vol. 54, no. 4, pp. 61–72, 2016.

[40] W. C. Zhu, J. Wei, J. Zhao, and L. L. Niu, "2D numerical simulation on excavation damaged zone induced by dynamic stress redistribution," *Tunnelling and Underground Space Technology*, vol. 43, pp. 315–326, 2014.

[41] X. J. Hao, S. H. Wang, D. X. Jin et al., "Instability process of crack propagation and tunnel failure affected by cross-sectional geometry of an underground tunnel," *Advances in Civil Engineering*, vol. 2019, Article ID 3439543, 17 pages, 2019.

[42] C. D. Martin, "Seventeenth Canadian geotechnical colloquium: the effect of cohesion loss and stress path on brittle rock strength," *Canadian Geotechnical Journal*, vol. 34, no. 7, pp. 698–725, 1997.

[43] R. S. Read and N. A. Chandler, "Minimizing excavation damage through tunnel design in adverse stress conditions," in *Proceedings of the 1997 World Tunnel Congress*, Vienna, Austria, 1997.

[44] Q. W. Wang, N. P. Ju, L. L. Du, and J. Huang, "Inverse analysis of geostress field in Bayu deep-buried tunnel on Lhasa-Linzhi railway," *Railway Engineering*, vol. 10, pp. 59–62, 2016, in Chinese.

[45] Y. Yang, D. Zhang, S. Li, L. Yang, and L. Jin, "In-situ stress test and rockburst analysis in Micang mountain tunnel," *Energy Sources Part A—Recovery Utilization and Environmental Effects*, vol. 2019, pp. 1–10, 2019.

[46] Y. L. Zhang, B. Y. Li, and D. Zheng, "Discussion on the boundary and area of the Tibetan Plateau in China," *Geographical Research*, vol. 21, no. 1, pp. 1–8, in Chinese.

[47] S. X. Yang, R. Yao, X. F. Cui, Q. C. Chen, and L. Y. Huang, "Analysis of the characteristics of measured stress in Chinese mainland and its active blocks and north-south seismic belt," *Chinese Journal of Geophysics-Chinese Edition*, vol. 55, no. 12, pp. 4207–4217, 2012.

[48] R. Yao, S. X. Yang, F. R. Xie, X. F. Cui, Y. Z. Lu, and Z. Y. Xu, "Analysis on magnitude characteristics of the shallow crustal tectonic stress field in Qinghai-Tibet plateau and its adjacent region based on in-situ stress data," *Chinese Journal of Geophysics-Chinese Edition*, vol. 60, no. 6, pp. 2147–2158, 2017.

[49] G. Kirsch, "Die theorie der elastizitat und die bedurfnisse der festigkeitslehre," *Zantralblatt Verlin Deutscher Ingenieure*, vol. 42, pp. 497–807, 1898.

[50] A. Bobet, "Lined circular tunnels in elastic transversely anisotropic rock at depth," *Rock Mechanics and Rock Engineering*, vol. 44, no. 2, pp. 149–167, 2011.

[51] A. Bobet, "Deep tunnel in transversely anisotropic rock with groundwater flow," *Rock Mechanics and Rock Engineering*, vol. 49, no. 12, pp. 4817–4832, 2016.

[52] A. M. Hefny and K. Y. Lo, "Analytical solutions for stresses and displacements around tunnels driven in cross-anisotropic rocks," *International Journal for Numerical and Analytical Methods in Geomechanics*, vol. 23, no. 2, pp. 161–177, 1999.

[53] S. A. Massinas and M. G. Sakellariou, "Closed-form solution for plastic zone formation around a circular tunnel in half-space obeying Mohr-Coulomb criterion," *Geotechnique*, vol. 59, no. 8, pp. 691–701, 2009.

[54] K. H Park, "Analytical solution for tunnelling-induced ground movement in clays," *Tunnelling and Underground Space Technology*, vol. 20, no. 3, pp. 249–261, 2005.

[55] F. Pinto and A. J. Whittle, "Ground movements due to shallow tunnels in soft ground. I: analytical solutions," *Journal of Geotechnical and Geoenvironmental*, vol. 140, no. 4, p. 17, 2014.

[56] S. K. Sharan, "Elastic-brittle-plastic analysis of circular openings in Hoek-Brown media," *International Journal of Rock Mechanics and Mining Sciences*, vol. 40, no. 6, pp. 817–824, 2003.

[57] O. E. Strack and A. Verruijt, "A complex variable solution for a deforming buoyant tunnel in a heavy elastic half-plane," *International Journal for Numerical and Analytical Methods in Geomechanics*, vol. 26, no. 12, pp. 1235–1252, 2002.

[58] O. P. M. Vitali, T. B. Celestino, and A. Bobet, "Shallow tunnels misaligned with geostatic principal stress directions: analytical solution and 3D face effects," *Tunnelling and Underground Space Technology*, vol. 89, no. 6, pp. 268–283, 2019.

[59] TB10621-2009, *Code for Design of High Speed Railway*, China Railway Press House, Beijing, China, 2009, in Chinese.

[60] B. S. Guan and Z. L. Guo, *Tunneling and Underground Engineering*, SouthWest JiaoTong University Press, Chengdu, China, 2000, in Chinese.

[61] Y. Y. Liu and M. H. Tang, *Rock Mechanics*, China University of Geosciences Press, Wuhan, China, 1999, in Chinese.

[62] W. D. Ortlepp and T. Y. Stacey, "Rockburst mechanisms in tunnels and shafts," *Technology*, vol. 9, no. 1, pp. 59–65, 1994.

[63] A. C. Adoko, C. Gokceoglu, L. Wu, and Q. J. Zuo, "Knowledge-based and data-driven fuzzy modeling for rockburst prediction," *International Journal of Rock Mechanics and Mining Sciences*, vol. 61, pp. 86–95, 2013.

[64] R. Shirani Faradonbeh and A. Taheri, "Long-term prediction of rockburst hazard in deep underground openings using three robust data mining techniques," *Engineering with Computers*, vol. 35, no. 2, pp. 659–675, 2019.

[65] E. Hoek and E. T. Brown, *Underground Excavation in Rock*, The Institute of Mining and Metallurgy, London, UK, 1980.

[66] N. Li and R. Jimenez, "A logistic regression classifier for long-term probabilistic prediction of rock burst hazard," *Nature Hazards*, vol. 90, no. 1, pp. 197–215, 2018.

[67] B. F. Russenes, "Analysis of rock spalling for tunnels in steep valley sides," M.Sc. thesis, Norwegian Institute of Technology, Department of Geology, Trondheim, Norway, 1974.

[68] I. A. Turchaninov, G. A. Markov, M. V. Gzovsky et al., "State of stress in the upper part of the Earth's crust based on direct measurements in mines and on tectonophysical and seismological studies," *Physics of the Earth & Planetary Interiors*, vol. 6, no. 4, pp. 229–234, 1972.

[69] S. D. Falls and R. P. Young, "Acoustic emission and ultrasonic-velocity methods used to characterise the excavation disturbance associated with deep tunnels in hard rock," *Tectonophysics*, vol. 289, no. 1–3, pp. 1–15, 1998.

[70] L. Zhou, Z. M. Zhu, and B. Liu, "Influence of cracks on surrounding rock damage-failure mode of straight wall arch tunnel," *Rock and Soil Mechanics*, vol. 38, pp. 3688–3697, 2017.

[71] H. Basarir, "Analysis of rock-support interaction using numerical and multiple regression modeling," *Canadian Geotechnical Journal*, vol. 45, no. 1, pp. 1–13, 2008.

[72] H. Basarir, M. Genis, and A. Ozarslan, "The analysis of radial displacements occurring near the face of a circular opening in weak rock mass," *International Journal of Rock Mechanics and Mining Sciences*, vol. 47, no. 5, pp. 771–783, 2010.

[73] X. M. Wang, L. J. Dong, and Y. H. Fu, "Prediction of possibility and the level of rockburst based on uncertain average gradted analysis method," *Science & Technology Review*, vol. 27, pp. 78–81, 2009.

[74] G. B. Zhao, D. Y. Wang, B. Gao, and S. J. Wang, "Modifying rock burst criteria based on observations in a division tunnel," *Engineering Geology*, vol. 216, pp. 153–160, 2017.

[75] J. Xing, J. B. Wang, L. Jiang, and X. B. Dong, "In-situ stress characteristics and rock burst prediction of the Guigala expressway tunnel," *Hydrogeology & Engineering Geology*, vol. 46, no. 2, pp. 170–178, 2019, in Chinese.

[76] W. Z. Zhang, "The regional geostress characteristics analysis and application in Dangjinshan tunnel," *Journal of Railway Engineering Society*, vol. 31, no. 12, pp. 18–22, 2014, in Chinese.

[77] F. L. Song and H. L. Zhao, "Study of key construction technologies of open TBM in complex geological conditions: a case study of Gaoligongshan tunnel," *Tunnel Construction*, vol. 37, no. S1, pp. 128–133, 2017, in Chinese.

[78] Y. S. Zhang, T. Xiong, Y. B. Du et al., "Geostress characteristic and simulation experiment of rockburst of a deep-buried

tunnel in Gaoligong mountain," *Chinese Journal of Mechanical Engineering*, vol. 28, no. 11, pp. 2286–2294, 2009, in Chinese.

[79] X. T. Feng, S. Y. Wu, Z. J. Li et al., "Comprehensive field monitoring of deep tunnels at Jinping underground laboratory (CJPL-II) in China," *Chinese Journal of Mechanical Engineering*, vol. 39, no. 1, pp. 356–366, 2016, in Chinese.

[80] S. Zhong, Q. Jiang, X. T. Feng et al., "Comprehensive field monitoring of deep tunnels at Jinping underground laboratory (CJPL-II) in China," *Rock Soil Mechanicas*, vol. 39, no. 1, pp. 356–366, 2018, in Chinese.

[81] L. S. Xu, L. S. Wang, Z. Y. Sun, and J. Xu, "In-situ stress measurement in rockmass of Erlang mountain highway tunnel," *Chinese Journal of Mechanical Engineering*, vol. 22, no. 4, pp. 611–614, 2003, in Chinese.

[82] P. Zhang, Z. G. Sun, Q. N. Wang et al., "In-situ stress measurement and the stability of surrounding rock in the north section of Muzhailing tunnel," *Journal of Geomechanics*, vol. 23, no. 6, pp. 893–903, 2017, in Chinese.

[83] Z. Song, C. B. Yuan, Y. B. Du, and Y. D. Wang, "The characteristics and formation mechanism of rock-burst for a long and deep tunnel of Chengdu-Lanzhou railway," *Journal of Railway Engineering Society*, vol. 34, no. 10, pp. 66–72, 2017, in Chinese.

[84] M. Gu, F. He, and C. Chen, "Study on rockburst in Qingling tunnel," *Chinese Journal of Mechanical Engineering*, vol. 21, no. 9, pp. 1324–1329, 2002, in Chinese.

[85] B. L. Song, "The analysis and discussion on the measured in-situ stress of drilling in the Qinling tunnel," *Journal of Railway Engineering Society*, vol. 4, pp. 54–59, 1996, in Chinese.

[86] X. M. Ma, H. Peng, J. S. Li, J. W. Li, and H. Q. Liao, "In-situ stress measurement and its application to rock burst analysis in Xinbaiyanzhai tunnel of the Xiangyu railway," *Acta Geologica Sinica*, vol. 27, no. 2, pp. 181–186, 2006, in Chinese.

[87] B. Z. Xiao, C. W. Luo, and Y. K. Liu, "In-situ stress measurement and prediction analysis of tunnel rockburst in west Hubei," *Chinese Journal of Mechanical Engineering*, vol. 24, no. 24, pp. 4472–4477, 2005, in Chinese.

[88] Y. J. Ma, C. W. Liu, F. Wu, and X. L. Li, "Rockburst characteristics and mechanisms during steeply inclined thin veins mining: a case study in Zhazixi Antimony mine, China," *Shock and Vibration*, vol. 2018, Article ID 3786047, 16 pages, 2018.

[89] R. D. Dwivedi, R. K. Goel, M. Singh, M. N. Viladkar, and P. K. Singh, "Prediction of ground behaviour for rock tunnelling," *Rock Mechanics and Rock Engineering*, vol. 52, no. 4, pp. 1165–1177, 2019.

[90] P. Jia and C. A. Tang, "Numerical study on failure mechanism of tunnel in jointed rock mass," *Tunnelling and Underground Space Technology*, vol. 23, no. 5, pp. 500–507, 2008.

[91] X. W. Xu, T. T. Guo, S. Z. Liu, G. H. Yu, G. H. Chen, and X. Y. Wu, "Discussion on issues associated with setback distance from active fault," *Seismol Geology*, vol. 38, no. 3, pp. 477–502, 2016, in Chinese.

[92] R. S. Yeats, K. E. Sieh, and C. R. Allen, *The Geology of Earthquakes*, Oxford University Press, New York, NY, USA, 1997.

[93] Q. Zhou, X. W. Xu, G. H. Yu, X. C. Chen, H. L. He, and G. M. Yin, "Width distribution of the surface ruptures associated with the Wenchuan earthquake: implication for the setback zone of the seismogenic faults in postquake reconstruction," *Bulletin of the Seismological Society of America*, vol. 100, no. 5B, pp. 2660–2668, 2010.

[94] C. Feng, Y. Yang, X. Ma, B. Qi, and P. Zhang, "Local stress perturbations associated with the 2008 Wenchuan M 8.0 earthquake near the Longmenshan fault zone in the eastern margin of the Tibetan plateau," *Journal of Asian Earth Sciences*, vol. 200, Article ID 104429, 2020.